Lifetime measurements of interference-narrowed sodium Stark resonances

P. McNicholl,* T. Bergeman, and H. J. Metcalf
Physics Department, State University of New York, Stony Brook, New York 11794
(Received 21 October 1987)

We report measurements of the temporal decay of sodium Stark resonances over regions of interference narrowing and compare with calculations using Wentzel-Kramers-Brillouin quantum-defect (WKB-QD) Stark theory. The measurements are performed with a beam of sodium atoms in a uniform electric field of ~ 3.2 kV/cm excited via the $3\,^2P$ state to ~ 285 cm^{-1} ($n^* \sim 20$) below the zero-field ionization threshold, and hence substantially above the classical saddle-point energy. For mixed states at level crossings, the discrete-continuum couplings interfere, yielding resonances that are stabilized against ionization over a small interval of the field. Measurements of the maximum lifetimes of $|m| = 1$ levels here are not limited by laser bandwidth, as were our previous spectral observations of $m = 0$ resonances. For three narrowing regions studied here, the observed maximum lifetime values of 127–191 nsec are 10–20% less than values obtained from WKB-QD calculations, while experimental error limits are $\sim 5\%$. After considering estimates for competing processes, namely radiative decay and transfer by blackbody radiation, a slight discrepancy remains.

I. INTRODUCTION

In 1985 we reported[1] very narrow features in the Stark spectrum of Na above the classical saddle-point energy, $E_{SP} = -2\sqrt{F}$. This narrowing was explained in terms of interference between the amplitudes for ionization into the various accessible continua. The measurements were found to agree in general with calculations performed with Harmin's Wentzel-Kramers-Brillouin quantum-defect[2] (WKB-QD) theory of the Stark effect, but observations of the extreme minimum width were limited by the pulsed-laser spectral resolution of about 1 GHz. We report here measurements of temporal decay rates that avoid this limitation. We have noted[3,4] previously generally very good agreement between experiment and theory even for these more stringent tests. However, we do find small discrepancies that are not easily explained by other possible effects.

Interference narrowing (or stabilization) of alkali-metal-atom Stark resonances was first observed in rubidium before the advent of Harmin's theory.[2] Feneuille *et al.*[5] found that in at least two instances, ionization lifetimes in rubidium increase and then decrease by a factor of greater than 30 over a small interval of the electric field. Subsequently, the reported energy-level structure and the lifetimes in these regions of stabilization have been found to agree generally with our WKB-QD calculations for rubidium, but the calculated maximum lifetime is more than twice the observed maxima. It is therefore of interest to investigate whether similar discrepancies occur in sodium, and to consider what other effects might contribute significantly to the observed decay rate.

Similar effects have been observed in cesium[6] at very high principal quantum number n and low electric field where the high density of quasibound Rydberg states served as the continuum. Other workers[7–10] have observed analogous effects in alkaline earths. Related phenomena also are found in nuclear and condensed-matter spectroscopy, and a special workshop devoted to the topic of stabilized states in the continuum was held in 1987.[11] Several theoretical discussions of stabilized states in the continuum have recently been presented.[12] The resonances reported here exhibit common features with resonances narrowed by interference in other contexts, but the particular circumstances in the Stark effect should be kept in mind.

For alkali-metal atoms at energies above the classical saddle-point ($E_{SP} = -2\sqrt{F}$) ionization in an electric field may be said to occur primarily by coupling between quasidiscrete hydrogenic basis states and continua. The coupling is produced by the nonhydrogenic part of the Hamiltonian, namely the ion core potential. When different Stark states are strongly mixed (for example, near an anticrossing), the ionization rate may be estimated from the properly weighted sum of the couplings between the components of the mixture and each of the accessible continuum states: there are circumstances where terms in this sum have opposite signs and therefore interfere. Then the ionization rate is reduced, often by several orders of magnitude, so as to produce very narrow spectral features. In certain cases, the core-induced width is canceled to such a degree that the dominant decay mechanism is ionization by hydrogenic tunneling, or by some other process such as radiative decay or transfer by blackbody radiation. We note, however, that the hydrogenic tunneling rate exceeds the core-induced ionization rate only in very limited field-energy regions, when a resonance happens to lie very near the parabolic critical energy (the top of the effective potential barrier for the given Stark channel).

The theory for alkali-metal Stark-resonance phenomena has been developed to a high degree of precision by Harmin[2] through the use of WKB methods and quantum-defect theory. In order to facilitate comparison with experiment we have recast the results of this theory in terms of a multicontinuum autoionization model.[13]

This model provides a definition of resonance energies and widths that is applicable even in regions of considerable intermixing and line-shape distortion. Therefore it becomes possible to extend maps of Stark-resonance energies to above the saddle point and on up to arbitrarily high field. Such maps will be presented here for the field-energy regions of interest. It is easy to locate regions of interference narrowing with this model. However, because there is some sacrifice in the ultimate accuracy attainable with the autoionization model, for all final comparisons made here with theory, resonance parameters were fit to the photoionization cross section calculated by Harmin's original methods.

II. EXPERIMENT

A. The apparatus

In our experiments a thermal Na beam collimated to about 0.01 rad is stepwise excited to Stark-Rydberg levels through the $3\,^2P$ state by sequential laser pulses in a dc electric field (see Fig. 1). The atomic beam is formed by a small stainless-steel oven heated to about 450 °C (monitored by a thermocouple) by a 100-W Fast Heat band heater. Its 0.3-mm aperture is about 100 mm away from a 0.7-mm movable aperture that serves both to define the beam and to separate the oven's vacuum chamber from the main chamber. The laser beams ($\sim$0.2-mm diameter at $1/e^2$ points) cross this atomic beam about 35 cm from the oven, thus defining the vertical angular spread of the excited atoms to be $\pm$0.003 rad.

The laser beams are formed by dye lasers and amplifiers pumped by a home-built nitrogen laser[14] that produces pulses of about 0.5-MW peak power and $\sim$8-nsec duration. The laser for the first excitation step from the ground $3\,^2S$ state to the $3\,^2P_{1/2}$ state at 589 nm serves little spectroscopic purpose and thus operates in two or three modes spread over 1–2 GHz. Its 22-cm-long cavity has internal lenses to reduce losses, and it is tuned by rotating a Littrow mounted grating that serves as a retroreflector for light diffracted by an intracavity grazing incidence grating[15] used for spectral narrowing. Its output goes to a single-cell amplifier whose light is intense enough to saturate and broaden the D-line transition.

Because the second excitation near 410 nm produces the signal, it must be more selective than the first one. In order to make this laser spectrally narrow, sweepable, and stable, it has been more carefully designed.[16] Its 5-cm-long cavity also has two gratings (but no lenses) on specially modified mounts to achieve the large free spectral range (3 GHz) that enables easy single-mode operation. Although a single mode is only about 200 MHz wide (Fourier transform limit is 40 MHz), pulse-to-pulse variations resulting from mechanical instabilities limit the effective bandwidth to about 600 MHz$=$0.02 cm^{-1}. This laser is also tuned by rotating the Littrow grating, but here the required smooth, uniform, repeatable movement is accomplished with a Burleigh Inchworm. We can scan the frequency about 20 cm^{-1} without a mode change. The output of this oscillator is amplified by two cells containing different dyes (DPS and LD425) whose gain profiles have opposite slope both to reduce stray light from amplified spontaneous emission and stabilize amplitude fluctuations. The pump light saturates these dye solutions to further stabilize the output power. This second laser beam is optically delayed from the first one by about 20 nsec and counterpropagates against it (for convenience only). Both laser beams are linearly polarized in the z direction (π light) and propagate in the $\pm x$

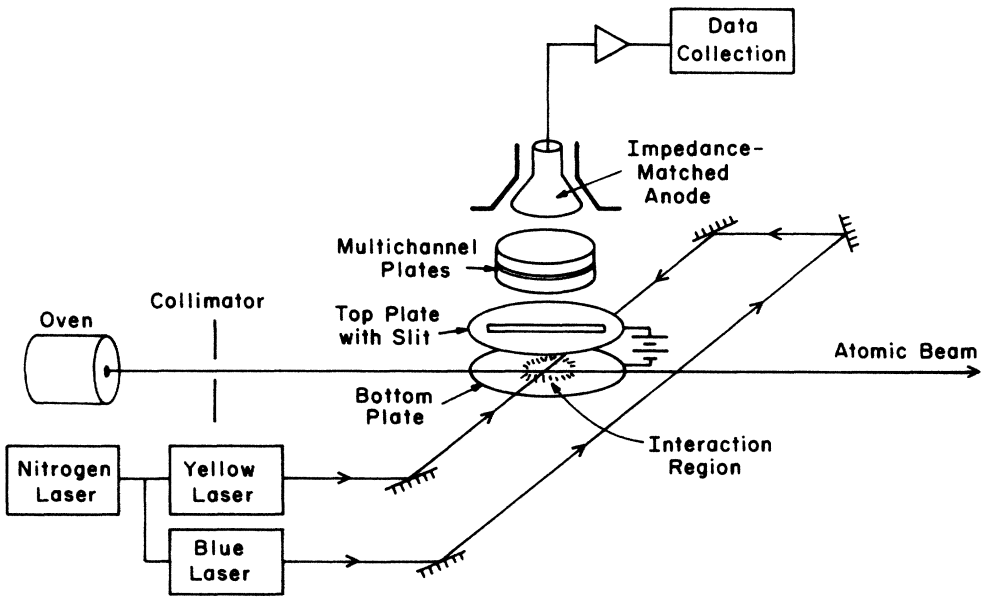

FIG. 1. Schematic diagram of the apparatus showing the atomic-beam arrangement and laser beams.

direction; the atomic beam propagates in the y direction.

The z-directed electric field is produced by a pair of oppositely charged parallel 3-mm-thick horizontal brass plates (machined and polished to about 0.001-in. flatness) on each side of the intersection of the laser and atomic beams. The lower one is smooth and solid but the upper one has a fine slit (0.25 mm by 25 mm) carefully aligned parallel to the atomic beam to allow photoelectrons to pass through it to a pair of multichannel detector arrays mounted just above it. The 75-mm-diam brass plates are separated by 7.24-mm Macor spacers machined and ground to achieve optimum parallelism (lengths equal to within ± 8 μm). The slit was chosen to minimize electric field inhomogeneities along the flight path of atoms in the beam. Inevitably, certain inhomogeneities do remain, and their effect on the results is discussed in Sec. II D. The voltage was produced by a Hewlett Packard HP6516A stabilized power supply, and the field was found to be stable to 10^{-4} during a data run by using the atoms themselves as probes. The voltage was measured with a HF3490A meter and a high-voltage probe, but the absolute field calibration was determined from the observed positions of the Stark resonances as compared with calculated values based on the known quantum defects of Na. Because the shifts relative to hydrogen Stark levels are typically less than 1 cm^{-1} in the field-energy region of interest, and because the quantum defect parameters are quite accurately known (see below), the calculated values for resonance field and energy are believed to be quite accurate. In view of the difficulty in measuring the plate spacing to comparable accuracy, no attempt was made to produce an "external" field calibration. Thus the only significant tests of WKB-QD Stark theory we consider here are for the extreme maximum lifetimes over regions of line narrowing.

The Galileo chevron multichannel plates were each operated with about 1 kV bias, and their output was collected on a carefully impedance-matched anode biased at 300 V. The result was a clean pulse easily transmitted on 50-Ω cable and amplified by standard linear pulse amplifiers.

In order to test for effects of the earth's field (which was not nulled), at one point in the data acquisition process, a magnetic field of 1 G (roughly twice the earth's field) was applied. There were no detectable effects on the observed lifetimes.

B. Measurements performed

In our first studies of interference narrowing[1] we measured the spectral width of various features by scanning the 410-nm laser and recording wavelength dependence of the photocurrent at various fixed fields. Details may be found in Refs. 1, 3, and 4. In some special cases we left the laser frequency fixed and swept the field through a resonance. But the resolution of each of these measurement techniques is essentially limited by the spectral width of the laser which meant we could not resolve widths narrower than about 600 MHz. This spectral resolution was sufficient for us to observe[1] interference narrowing in $m=0$ levels to an appreciable degree because the normal width (at ~ 4 kV/cm, 200 cm^{-1} below the zero-field ionization threshold) is 2–3 cm^{-1}. For a given field and energy in sodium, $m=0$ resonances have the greatest width because the s component leads to the largest core overlap, hence strongest coupling with continuum states. However, the calculated $m=0$ minimum ionization width of 200 MHz could not be verified because it was less than our spectral resolution.

In order to probe minimum widths produced by interference narrowing, we undertook direct measurements of the decay lifetime of longer-lived states by recording the time dependence of the signal. Such measurements on $m=0$ states would be very difficult at the field-energy region that is convenient for our experiments. Their minimum width of ~ 200 MHz corresponds to a maximum decay time of less than 1 nsec, while the pulse duration of our excitation lasers was about 6 nsec. In order to make good measurements of changes in the decay time we require lifetimes of at least 10–15 nsec and observation intervals a few times longer than this. On the other hand, because the average speed of thermal Na atoms is about 1 mm/μsec, and because the field inhomogeneities were significant over distances of about 1 mm, the decay-time measurement is limited to a dynamic range of about a factor of 50. We therefore chose $m=1$ states and an energy domain closer to the saddle point so that the maximum decay time was consistent with the temporal resolution of our apparatus. Figure 2 presents a plot of sodium Stark-resonance energies for energies near the narrowing regions studied here, which are contained within the two boxes. At zero field, levels converge to $n=20$, $L \geq 2$ at -274.34 cm^{-1} and to $21\,^2P$ at -270.41 cm^{-1}. A dotted line denotes the classical saddle-point energy, above which Stark levels successively pass over their respective thresholds, and broaden into continua. Although this broadening takes place over a range of field values, the nominal threshold (the "parabolic critical en-

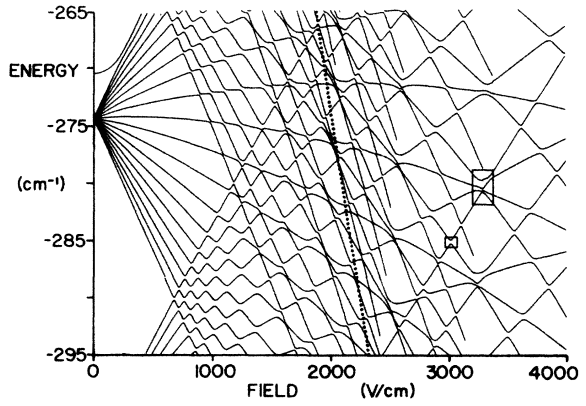

FIG. 2. Sodium Stark resonance energies calculated with the multichannel formulation of WKB-QD Stark theory (Ref. 13). The stabilized states studied in the present work lie in the two boxes, which are magnified in Figs. 5 and 9(b). The levels shown at zero field have quantum numbers $n=20$, $L \geq 2$, and $21\,^2P$. The dotted line is the classical saddle-point energy. The plotted line for a resonance terminates when the corresponding hydrogenic level passes over its respective threshold, the parabolic critical energy.

ergy" for the given channel) lies where the plotted line terminates. The energies plotted are actually the real part of the eigenvalues of a complex symmetric matrix whose elements are obtained from WKB-QD Stark theory by use of a multichannel autoionization model, as discussed in Ref. 13. The level repulsion due to mixing of hydrogenic Stark states by the sodium ion core is evident in this figure and in the more detailed figures below.

C. Nature of the signals obtained

In order to reduce the effects of field inhomogeneity seen by the decaying atom along its flight path, we chose a data collection scheme that would be relatively independent of such effects. We first excite a long-lived mixture of states at a particular energy E and field F, let it evolve (decay) for a fixed time T, and then make a small (15–25 V/cm) but fast change in the field by applying a 10–15 V pulse to the field plates. If the conditions are properly chosen stabilization does not occur in this new field, so the remaining atoms decay very quickly.

The resulting signal is a slow exponential[17] decay terminated by a large pulse $S(F,T)$ whose area is proportional to the number of atoms that survived in their excited state from the laser pulse until the voltage pulse. Some examples are shown in Fig. 3. This pulse is fed to an appropriately delayed, gated integrator whose output is digitized and then summed with others in a signal averager whose horizontal axis is the delay time T. To evaluate the expected signal, we first note that the pulse height is

$$S(F,T)=S_0\exp[-\Gamma(F)T] , \tag{1}$$

where $\Gamma(F)$ is the decay rate at field F. Near the field of maximum interference and therefore minimum Γ, we can make the approximation[18]

$$\Gamma(F)\cong\Gamma_0(1+X^2) , \tag{2}$$

where $X=(F-F_0)/\Delta F_0$, F_0 is the field where Γ takes on its minimum value Γ_0, and ΔF_0 is a field parameter to be determined experimentally and compared with theory. We then find that $S(F,T)$ decreases exponentially with time T and is a Gaussian in field F centered at $F=F_0$ of half width at half maximum (HWHM) $\sigma_0=\Delta F[(\ln 2)/\Gamma_0 T]^{1/2}$,

$$S(F,T)=S_0\exp(-\Gamma_0 T)\exp(-\Gamma_0 T X^2) . \tag{3}$$

Although the fidelity of a time scan would be compromised by the flight of atoms through differing field inhomogeneities, a field scan is less compromised by this effect because the time of flight for all atoms has the same distribution with T fixed. A three-dimensional plot of the dependence on both field and time is shown in Fig. 4.

We begin with a discussion of temporal measurements in one of several regions of line narrowing near where four levels approximately cross. The four resonances are identifiable by hydrogenic quantum numbers $(n,n_1,m_L)=(18,16,1)$, (19,12,1), (20,9,1), and (21,7,1), and they converge near $E=-280\ \text{cm}^{-1}$ and $F=3280$ V/cm, as shown in the larger box in Fig. 2 and in more detail by the computational results presented in Fig. 5, also obtained with the multichannel autoionization formulation of WKB-QD Stark theory.[13] The calculated decay rates for the resonances in Fig. 5 are plotted in Fig. 6. For this four-level crossing region, there are six regions of line narrowing (the number of distinct pairs of four levels) marked by circles in Fig. 5. The two cases studied experimentally here are denoted B and C. The normal decay rate for $|m_L|=1$ levels in this region is indicated by the top curve in Fig. 6, which corresponds to a width of $0.1-0.3\ \text{cm}^{-1}$.

First we discuss measurements in the region labeled C in Fig. 5. Figure 7 shows three data sets that measure the time dependence of $S(F,T)$ at different fields and the associated fitted values of the lifetime $\tau(F)\equiv 1/\Gamma(F)$. In Fig. 8 we plot measured values of $\tau(F)$ versus F. The

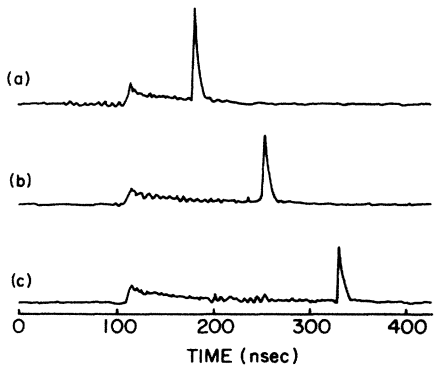

FIG. 3. Pulsed-induced decay at the level crossing A in the small box of Fig. 2 and shown in detail in Fig. 9. The stabilized state is seen to decay freely for (a) 75, (b) 150, (c) 225 nsec at which time a 10–15-V pulse takes the atom beyond the stabilizing field so that the decay rate increases abruptly, resulting in prompt decay of all remaining atoms.

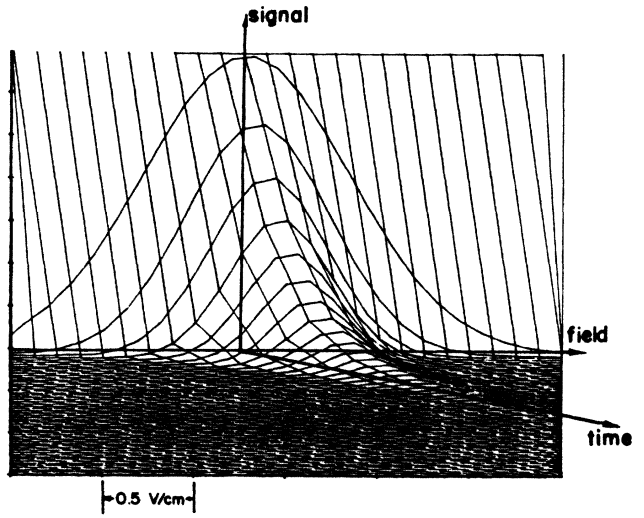

FIG. 4. A three-dimensional representation of the field and time dependence of the ionization rate near a point of interference stabilization. At the proper field, the lifetime is longest, resulting in a long decay time.

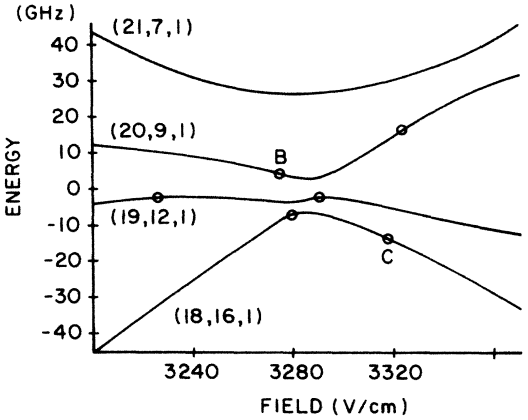

FIG. 5. An enlargement of the larger boxed region of Fig. 2, showing narrowing regions denoted by B and C in the text. The zero of energy scale corresponds to 280.3 cm^{-1} below the zero-field ionization threshold. Minima in the ionization rate are indicated by circles.

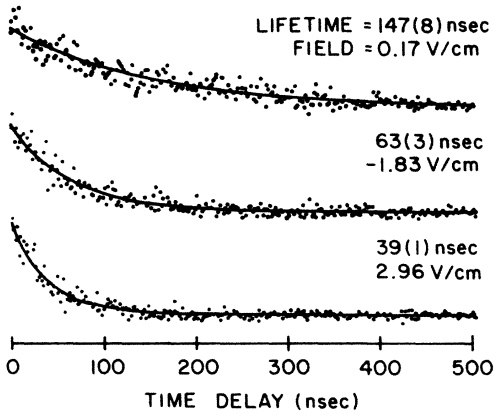

FIG. 7. Results of the time delay scans for crossing C at three different fields. The field values given are relative to the fitted crossing center and the lifetimes are those obtained by a fit to an exponential form. The solid lines are the plots of the fitted decay curve.

long-dashed line shows the best-fitted Lorentzian. The solid line shows the values calculated with WKB-QD Stark theory, and the short-dashed line shows the theoretical values with the field inhomogeneity folded in, as discussed in Sec. II D below. The difference between the curves will be discussed later.

These measurements in region C of Fig. 5 have been fitted with Eq. (3) which assumes that the field seen by all the atoms is the same and is constant. The neglect of field inhomogeneities is justifiable in this case because the measured field variation over the experimental region is only ~ 0.2 V/cm and the width ΔF_0 of the narrowing curve is about 3.5 V/cm. By contrast, the narrowing curves in other regions are not as broad, and the field inhomogeneities have a significant effect. Figure 9 shows the observed, theoretical, and convoluted theoretical lifetime values for region A. In this case, the width of the crossing region is less than 0.8 V/cm, so the effect of field inhomogeneity, seen as the difference between the solid line and the short-dashed line, is more important.

D. Effect of the field inhomogeneities

In several respects, the presence of the slit in the upper electric field plate modifies the ideal of a uniform field and uniform detectability over space. First, electrons will be detected only from atoms ionized directly below the slit. Since the detection region beneath the slit is long and narrow, misalignment of the slit and atomic beam allows some excited atoms to pass out of this detection region before they decay. We estimate that this misalignment can be no more than 4°, providing a transverse velocity of 70 m/sec for thermal atoms moving at 10^3 m/sec, hence a transverse displacement of 14 μm during a decay lifetime of 0.2 μsec. Thus, with a 4° misalignment, 6% of the atoms will pass out of the 220-μm-wide

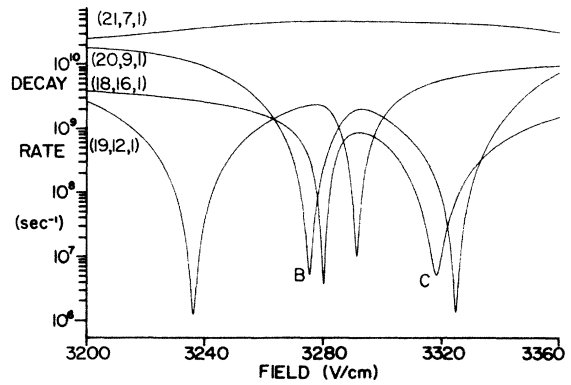

FIG. 6. Decay rates for the four energy levels plotted in Fig. 5. As for the previous figure, the hydrogenic quantum numbers given apply only to the low-field side of the figure. At higher fields, there is extensive mixing and transformation of character. The maximum decay rate plotted corresponds to a width of 0.3 cm^{-1}.

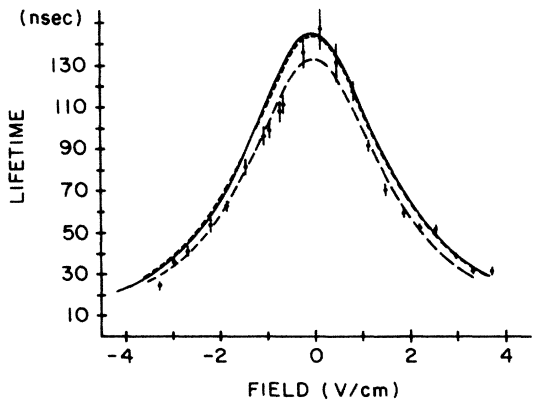

FIG. 8. Experimental (data points) and theoretical (solid line) lifetimes vs field for crossing C. The short-dashed line indicates the expected effect of the field nonuniformity on the theoretical curve, and the long-dashed line represents a fit to the data.

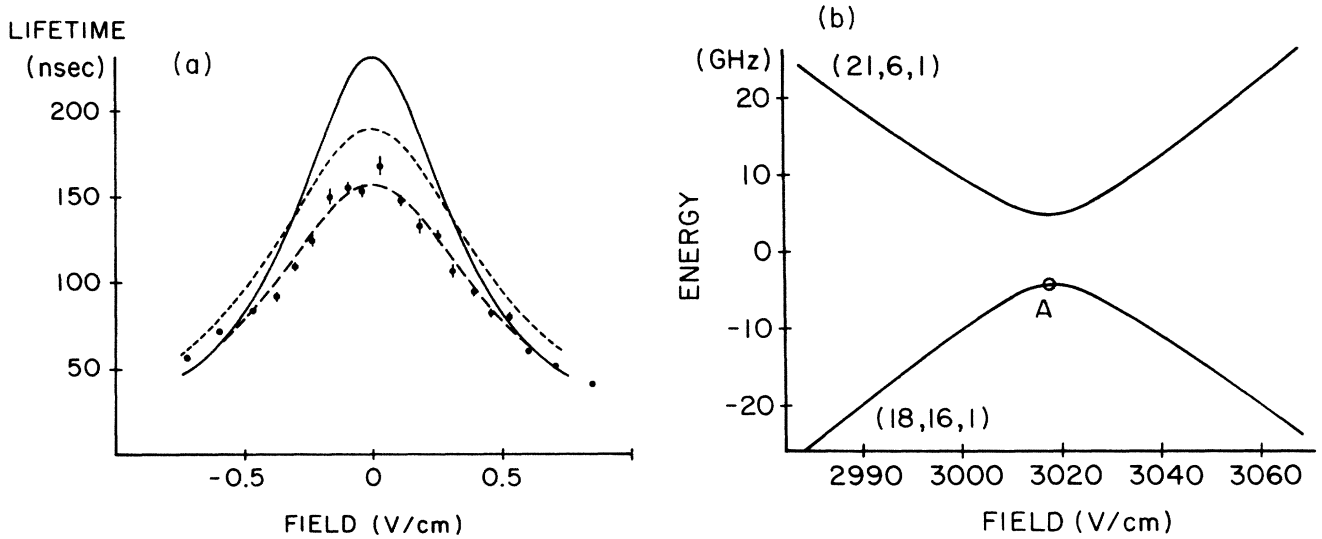

FIG. 9. (a) Same as for Fig. 8, but for crossing A. The effect of field inhomogeneity is more important here because the narrowing occurs over a much smaller interval of the field. (b) Magnification of the small boxed area of Fig. 2 which shows the energy levels. The zero of energy here is $-285.11\ \text{cm}^{-1}$.

detection region during one lifetime. No observable effect is to be expected, however, since an equal number of excited atoms pass into the detection region during this time.

Second, the field inhomogeneity from the slit causes the field seen by an atom to change slightly along its flight path and also causes different atoms to see different field values. To estimate the effects arising from the field nonuniformity, we have calculated the spatial variation of the field using eigenfunction expansion methods in two dimensions, and also we have experimentally estimated the field inhomogeneity from analysis of temporal decay versus field as described below. Furthermore, the field nonuniformity produced by these particular electrode plates has been studied separately by Yang,[19] subsequent to the data acquisition and analysis discussed here. The conclusion from the two experimental approaches is that the predominant variation of the field is in the vertical direction and amounts to a field gradient of about 15 V/cm^2 midway between the plates. The field is found to *increase* as one approaches the slot. By contrast, the field calculated for an ideal slot decreases near the slot, and is found to have a field gradient midway between the plates of less then 2 V/cm^2. Yang[19] has further determined that the observed inhomogeneity is due to a lip, or raised portion, on the edge of the slot produced in the machining process. This raised portion is maximum at the center of the plate and decreases in either direction along the slot, thereby producing a field maximum along the atomic beam at the center of the plates, as reported in Sec. II F. This interpretation was derived from electric field mapping procedures not available at the time of the original data acquisition and analysis. However, the data analysis described below was conducted in such a way as to deal with this type of field inhomogeneity.

Midway between the plates, the variation of the field in the transverse direction over the detection region is estimated to be insignificant. However, the measured vertical gradient of the field implies a total vertical change of 0.3 V/cm over the 0.2-mm diameter of the laser beam. Since the field varies approximately linearly over the laser beam, the weighted distribution of field values seen by atoms over the laser beam is approximately Gaussian, following the laser-beam profile.

We first consider the effect of the field change an atom sees during its lifetime due to the vertical variation of the field. We find the vertical velocity spread geometrically from the 0.3-mm-oven aperture and 0.7-mm aperture 10 cm away to be ± 10 m/sec. However, if the plate is inclined relative to the beam by 0.02 rad, then the additional vertical velocity relative to the plate of the plate is 20 m/sec, leading to a field change over the 0.2-μsec decay lifetime of ~ 0.006 V/cm. This corresponds to a small fraction of the narrowed HWHM even for case A, hence is not a likely source of possible errors.

The primary effect of atoms moving into a field for which the decay rate changes is a shift of the lifetime versus field function by an amount that depends on the delay time. Since no appreciable asymmetry in the decay function with delay time was noted, we estimate that this effect would change the maximum lifetime by less than 1%.

By far, the most significant effect of field inhomogeneity is the distribution of field values seen by different atoms in the laser beam beneath the slit. We model this effect with a Gaussian distribution (width ΔF_I) of field values seen by different atoms whose paths are parallel to the slit but displaced from one another. Then the expression for our observed signal becomes the simple convolution

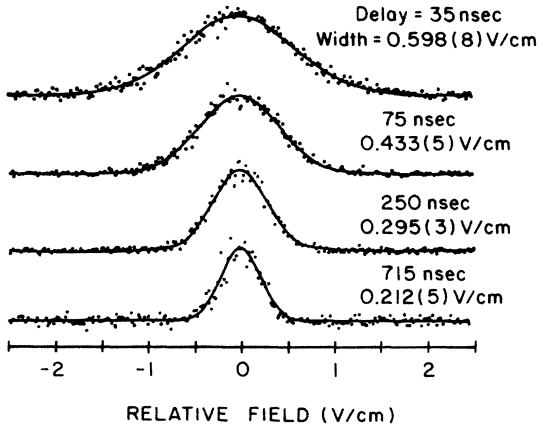

FIG. 10. Typical data for field scans at various time delays for region A of Fig. 9. The solid lines represent fitted Gaussian curves, for which the corresponding widths are given, with statistical uncertainties.

$$S(F,T,\Delta F_I)=\int dF' S(F',T) \times \exp[-(F'-F)^2/\Delta F_I^2]/\Delta F_I\sqrt{\pi}$$
$$=[S_0\Delta F_0/(\Delta F\sqrt{\Gamma_0 T})]\exp(-\Gamma_0 T) \times \exp(-X_I^2)\,, \quad (4a)$$

$$\Delta F^2=\Delta F_I^2+\Delta F_0^2/\Gamma_0 T\,, \quad (4b)$$

where $X_I \equiv (F-F_0)/\Delta F$. Unless ΔF_I is very much smaller than ΔF_0, $S(F,T,\Delta F_I)$ is not exponential in T, and it is very difficult to separate the effect of inhomogeneity from that of narrowing. On the other hand, the Gaussian signal that results from fixing T and scanning the field has a width that depends on T in a simple way as given in Eq. (4b), and a fit of the measured width versus T can be used to extract a value for the inhomogeneity width ΔF_I.

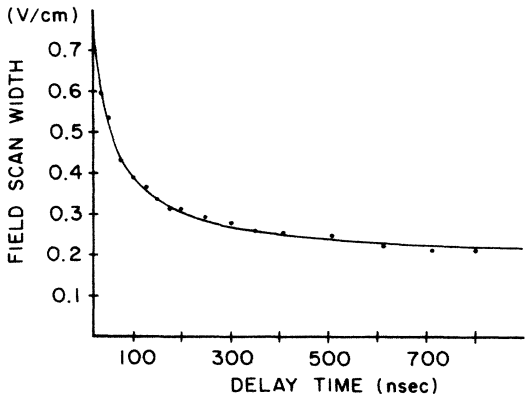

FIG. 11. Width of the field scans of Fig. 10 vs delay time. The experimental points have been fitted by Eq. (4b) (solid curve) and the experimental parameters have been extracted from the fit.

E. Lifetime results

In Fig. 10 we show field scans at fixed laser frequency for several values of T in region A of Fig. 9(b), and we have plotted the observed (fitted) width versus T in Fig. 11. We have then fitted Eq. (4b) to this and also to a similarly derived curve from region B of Fig. 5, and extracted values for both ΔF_I and $\Delta F_0/\sqrt{\Gamma_0}$ for each case. We then used these values of ΔF_I and $\Delta F_0/\sqrt{\Gamma_0}$ as fixed parameters to determine Γ_0 from temporal measurements of these same spectral features, as described above. The results are presented in Table I, along with calculated values for comparison.

Effects of the Stark shifts of the levels that occur in field scans are included by using the theoretical values of the Stark coefficients and assuming a Gaussian spectral shape for the laser. We found that these corrections were small enough to allow us to determine experimentally that the effective laser width was about 500 MHz. This is consistent with other measurements, and quite adequate for interpretation of our field scans.

F. Mapping the field

By steering the laser beams and thereby displacing the interaction region in the apparatus, we have exploited the very high sensitivity of these measurements to map the electric field in the longitudinal direction. This is the first time that spatial mapping of an electric field has been accomplished to such high precision and resolution with a technique that has so much potential for use over a wide range of field magnitudes.

In Fig. 12 we plot the varying voltage required to produce the appropriate F_0 for region A of Fig. 10 with a 200-nsec delay as a function of longitudinal position (y direction) along the slit, measured from its center. The three data sets are taken along three horizontal lines at different heights (i.e., different values of z) above the lower plate, and show clearly that the field is most uniform nearest this solid plate, as might be expected. (The vertical dependence of the field at the center was not accurately monitored and therefore differs for the three curves in an undetermined way.) Note that, for reasons discussed in Sec. II D, the field is maximum at the center of the slit. It is clear from Fig. 12 that the variation of field along the slit will have a negligible effect on our lifetime measurements if the excitation takes place near the center of the slit.

G. Interference of dipole transition strengths

The superposition states that result from mixing by the field are stabilized against decay because the discrete-continuum coupling elements destructively interfere. Analogous interference effects can also cause cancellation in the amplitude for other processes, such as electric dipole transitions, as observed previously.[20–22] In the present study we also observe this phenomenon. Figure 13(a) shows a series of laser scans at different field values near region A of Fig. 9. The narrowing effect is visible here, but is not very noticeable because of the limits imposed by the laser resolution. Much more dramatic is the

TABLE I. Results of measurements and calculations on the narrowing regions labeled A, B, and C. ΔF_0 is the width of the crossing region as defined below Eq. (1). ΔF_I is the fitted field inhomogeneity parameter, not determined for case C because the large value of ΔF_0 made the data insensitive to it. Γ_0 and τ_0 are the minimum decay rate and maximum lifetime, Γ_{dif} is the rate needed to account for the discrepancy between observation and theory. Error limits given in parentheses for the calculated values represent solely the effect of uncertainties in the fitted quantum-defect parameters (see text).

	Narrowing region		
	A	B	C
ΔF_0 (V/cm)			
Expt.	0.357(16)	0.747(46)	1.75(9)
Calc.	0.373	0.765	1.79
ΔF_I (V/cm)			
Expt.	0.184(4)	0.222(8)	
τ_0 (nsec)			
Expt.	191(11)	127(7)	134(7)
Calc.	232(1)	143.6(2)	146.0(1)
Γ_0 (10^6 sec^{-1})			
Expt.	5.24(30)	7.87(46)	7.48(40)
Calc.	4.32(2)	6.96(1)	6.849(5)
Γ_{dif} (10^6 sec^{-1})	0.92(30)	0.91(46)	0.63(40)

disappearance [Fig. 13(b)] of the excitation oscillator strength of one of the interfering components about 14.5 V/cm below the center of the anticrossing. Figure 13(b) also clearly shows the reversal of the asymmetry of the Fano profile that arises because of the sign change of transition amplitude relative to that of the direct ionization amplitude.

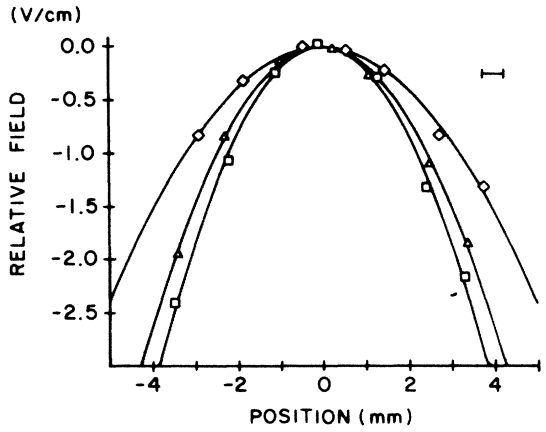

FIG. 12. Field nonuniformity in the longitudinal direction. The apparent displacement of the resonance is plotted as a function of the displacement of the interaction region from the center of the electrode slit. The data were taken for case A, so the field is 3018.29 V/cm. The three sets of data were taken at 1-mm vertical spacings. The diamonds denote those at 1 mm from the lower electrode, the triangles at 2 mm, and the squares at 3 mm. Only the relative field along the longitudinal direction is indicated; the relative field values at the center for the various vertical positions could not be monitored. The solid lines are the results of quadratic fits to the data. The error bar shows the uncertainty in the measured position of the laser–atomic beam intersection point.

III. COMPARISON BETWEEN EXPERIMENTAL AND THEORETICAL RESULTS

Table I summarizes the experimental and theoretical results for regions A, B, and C. We give values for the width of the narrowing region ΔF_0 [Eq. (2)], the fitted field inhomogeneity ΔF_I [Eq. (4)], and the maximum lifetime (inversely, the minimum decay rate). The uncertainties (one standard deviation) quoted for the experimental quantities in Table I are purely statistical, from the least-squares fits. The difference in ΔF_I values quoted for regions A and B is due primarily to a realignment of the laser between the acquisition of the two sets of data. It thus reflects the sensitivity of this parameter to the location of the interaction region between the slotted and blank electrode. Γ_{dif} is the difference between the theoretical and experimental values and will be compared below with estimated rates of decay processes other than ionization.

The theoretical values for the minimum decay rate were obtained from fits to photoionization line shapes calculated with WKB-QD Stark theory, using computer codes written by Harmin[23] and modifications thereof. We have performed calculations neglecting spin-orbit effects and also with ^2P and ^2D spin-orbit splittings included, using a multichannel version of WKB-QD Stark theory.[24] In order to obtain convergence for cases A and B, it was necessary to include quantum defects for L equals 1 up to 6 ($L=0$ is not needed for $m=1$ states). The quantum-defect values needed were obtained[13] for $L=1-5$ by fitting optical[25] and microwave[26,27] data combined with appropriate weights, while for $L=6$, they were obtained from the effective polarizability of the sodium-ion core according to relations given by Freeman and Kleppner.[28] The ^2D fine-structure splitting was extrapolated from the measurements of Salour.[29] A two- or

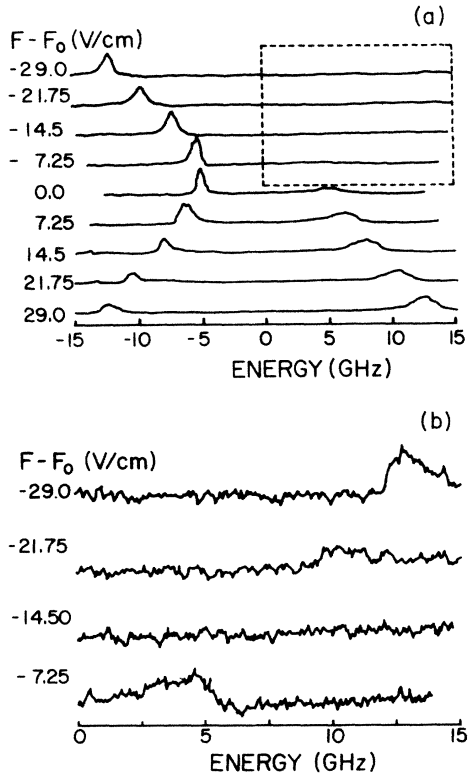

FIG. 13. (a) Spectral scans in region A of Fig. 9 at various values of the field relative to F_0, the field for the lifetime maximum. The spectral narrowing of the left peak due to interference in the ionization process is evident. More important here is the vanishing of the signal along the right side because of interference of the dipole transition matrix elements. (b) Detail, at higher gain, of the boxed region of (a), showing the reversal of the asymmetry of the line shape.

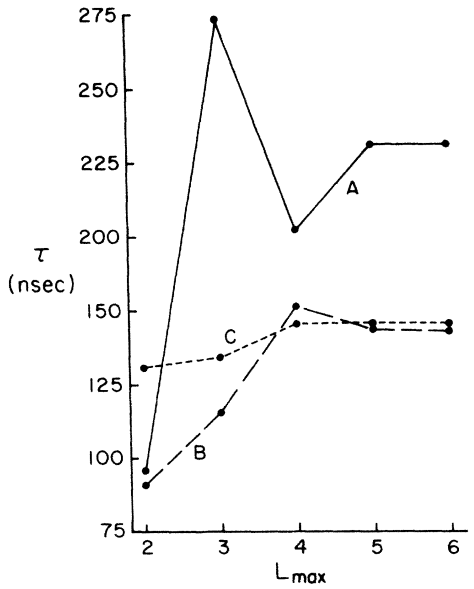

FIG. 14. Calculated maximum lifetimes for the three stabilizing regions as a function of the maximum L value for which the quantum defect was assumed to be nonzero. The surprising sensitivity to high-L values arises because low-L effects are canceled by interference. The differences between the two spin components are negligible on the scale of this graph.

three-term expansion in powers of the binding energy was used in fitting the data. The δ_L values at -285 cm^{-1} (fine structure omitted), together with the statistical uncertainties propagated from the fits, are 0.855 320(2), $1.4803(7)\times10^{-2}$, $1.609(5)\times10^{-3}$, $4.28(2)\times10^{-4}$, $1.52(2)\times10^{-4}$, and $6.44(10)\times10^{-5}$. The $^2P_{1/2}$ and $^2P_{3/2}$ difference is $8.07(2)\times10^{-4}$, while the $^2D_{3/2}$-$^2D_{5/2}$ difference is $-1.4(1)\times10^{-5}$.

The maximum lifetimes over each of the narrowing regions A, B, and C are plotted in Fig. 14 as a function of the maximum L included in the calculation. (The field at which the maximum calculated lifetime occurs depends slightly on $L_{\max}$.) The error limits given with the calculated values in Table I represent solely the effect of uncertainties in the fitted quantum-defect values. At present, we do not have a means of estimating the possible errors introduced into the calculated values due to use of the WKB approximation.

The two $|m_L|=1$ fine-structure levels ($|m_J|=\frac{1}{2}$ and $\frac{3}{2}$) at the respective points of maximum lifetime are found to differ very little in energy and lifetime. The energy splittings are found to be 0.36, 0.09, and 0.024 MHz for cases A, B, and C, respectively. This may be compared with the 20 ^2P fine-structure interval of 757 MHz, the 20 ^2D interval of -11.5 MHz, and with the minimum linewidths for regions A, B, and C of 0.7, 1.1, and 1.1 MHz, respectively. Normally one would expect on average that an $n=20$ Stark level would exhibit a fine-structure splitting of one-twentieth of the zero-field 20 ^2P splitting, the ^2D state splitting being negligible by comparison. The calculated values are much less than this because (a) the stabilized states have very little p character (minimal core overlap for $|m_L|=1$) and (b) the D state fine structure cancels most of the remaining P state effect. For similar reasons, the differences for the maximum lifetimes between the two fine-structure components for cases A, B, and C are calculated to be only 0.04%, 0.08%, and 0.01%, respectively. We conclude, therefore, that spin-orbit effects are negligible compared with experimental uncertainties.

It is clear that there is generally good agreement between measured ionization lifetimes and WKB-QD theory. Calculated values for ΔF_0 are within the estimated error limits of the experimental values. However, for Γ_0 there are discrepancies of up to 20% that are larger than the combined effects of measurement error limits and the uncertainties in the empirical quantum defects. Several possible explanations for the discrepancies in the Γ_0 values can be proposed.

(a) Perhaps the modeling of the field inhomogeneities is somehow inadequate. This is consistent with the conclusion that the largest (smallest) discrepancy occurs for case A (C), which is most (least) sensitive to field inhomogeneities. To the extent of our understanding, the single

effect that may be significant at the 1% level but which was not considered in the data analysis is a slight variation of the field seen by the decaying atom if there is a vertical velocity component in the presence of the field gradient due to the slit. As stated in Sec. III D, to first order, such an effect would produce an asymmetry in the decay curve as a function of the time delay. Although no such parameter was included in the fitting procedure, this effect was not evident in the residuals.

(b) Another decay process may account for the difference in Γ_0 values. In fact transfer by blackbody radiation and also radiative decay are expected to occur to some degree. There are two difficulties with this explanation. First, the addition of a constant decay term would imply, by Eq. (2), that ΔF_0 would also be affected, whereas in each case ΔF_0 is in good agreement with theory. Second, the required rates, given by $\Gamma_{\rm dif}$ in Table I, exceed estimates based on previous work.

For blackbody radiation at zero field, Cooke and Gallagher[30] obtain a rate

$$\Gamma_b = (6.79\times 10^4) T/n^{*2}\ \sec^{-1}\ ,$$

which is independent of L. If the rate is truly L independent, it would be unaffected by mixing in the electric field. Farley and Wing[31] have explicitly calculated blackbody transfer rates for sodium $L=0$–3 Rydberg levels, and find them slightly less than the above value, with a small-L dependence. We conclude that at $T=300$ K, $E=-285\ \text{cm}^{-1}$ ($n^*\cong 20$), a rate $\Gamma_b = 5.2\times 10^4\ \sec^{-1}$ from the above expression is a reasonable upper bound.

For the radiative decay rates, estimates for sodium can be based on the rates calculated for specific hydrogen Stark levels at zero field by Hiskes, Tartar, and Moody.[32] Radiative lifetimes of sodium nL levels at zero field are less than in hydrogen for $L=0$, but much greater for $L=1$, slightly greater for $L=2$, and comparable to the hydrogenic values for $L>2$.[33,34] Our own estimates of the effect of the electric field on radiative lifetimes of hydrogen Stark sublevels indicate that the levels of highest n_1 for a given n manifold decay more rapidly than at zero field by as much as 25%, while upward-going levels of smaller n_1 are less affected by the field. For $n=18$ to 21 (the hydrogen values are independent of n_1 for $|m|>0$) one reads values from the graph of Ref. 32 of 18-33 μsec, corresponding to rates of 3.0 to $5.6\times 10^4\ \sec^{-1}$. Thus the approximately equal blackbody transfer and radiative decay rates sum to no more than about $1.2\times 10^5\ \sec^{-1}$, which is too small to account for the discrepancies in the observed decay rates.

It is conceivable that interference effects could occur in a single dominant branch in the radiative decay rates. There might even be an appreciable variation of the radiative decay rate over the narrowing region so as to account for the observed ΔF_0 values. In any case, it would be useful to have more reliable estimates for blackbody transfer and particularly radiative decay in the presence of an electric field.

(c) A third possible significance of the discrepancies is that the rates calculated by WKB-QD Stark theory for the stabilized states are slightly in error. Because of the high degree of interference cancellation, these measurements represent a very stringent test of the theory. For hydrogen, WKB widths have been found to agree with "exact" numeric calculations to better than one part in 10^4. For alkali-metal atoms, there is good agreement on a very diverse set of comparisons with experimental line shapes, resonance energies, and widths. At present, therefore, we regard this at the least likely explanation.

IV. CONCLUSION

"Stabilized" Stark resonances are fascinating because the reduction in ionization decay rate occurs by a large factor over a very small interval of the electric field. Our calculations with WKB-QD Stark theory[2] and variations thereof[13] indicate that line narrowing or stabilization occurs very generally in sodium in regions where two or more hydrogenic levels cross. In this work, we have studied one case of a stabilized state in a two-level crossing, and two cases out of six stabilized states in a four-level crossing.

Because the field dependence of interference narrowing is so sharp, there is the obvious possibility of using the anomalously long lifetime for a precise electric field calibration. The HWHM of the narrowing region ($\Delta F_0/F_0$) was as small as 1.2 parts in 10^4. The observed lifetimes of 134-191 nsec represent an increase by factors of 10^3 to 10^4 over the "normal" lifetime of 0.02-0.10 nsec (corresponding to linewidths of 0.5-0.3 cm^{-1}) for the $|m|=1$ levels studied here (field-energy region 3.3 kV/cm, 285 cm^{-1} below the zero-field ionization threshold).

Because of the complicated pattern of interference among the discrete-continuum coupling elements, stabilized states present very sensitive tests of theory. It is remarkable that the location and magnitude of the lifetime peak were quite well predicted by WKB-QD Stark theory. The true limits of accuracy of this theory are difficult to establish. Our measurements of the extent of lifetime stabilization are all within 20% of theory. However, the discrepancies between experiment and theory for the maximum lifetime are 1.5 to 3.0 times the estimated experimental error. Our best estimates for the rates of transfer by thermal blackbody radiation and for radiative decay reduce the discrepancies to 1.3 to 2.6 standard deviations. Before one can say whether the theoretical minimum ionization rates are significantly in error, the rates for these competing decay processes in the presence of an electric field (most especially that for radiative decay) need to be more reliably estimated.

ACKNOWLEDGMENT

This research was supported by the National Science Foundation.

*Present address: Photometrics Inc., 4 Arrow Drive, Woburn, MA 01801.

[1]J.-Y. Liu, P. McNicholl, D. A. Harmin, J. Ivri, T. Bergeman, and H. J. Metcalf, Phys. Rev. Lett. **55**, 189 (1985).

[2]D. A. Harmin, Phys. Rev. A **24**, 2491 (1981); **26**, 2656 (1982).

[3]P. McNicholl, Ph.D. thesis, State University of New York at Stony Brook, 1986.

[4]P. McNicholl, T. Bergeman, and H. J. Metcalf, in *Spectral Line Shapes*, edited by R. J. Exton (Deepak, Hampton, VA, 1987), Vol. 4.

[5]S. Feneuille, S. Liberman, E. Luc-Koenig, J. Pinard, and A. Taleb, J. Phys. B **15**, 1205 (1982).

[6]C. Chardonnet, D. Delande, and J.-C. Gay, Opt. Commun. **51**, 249 (1984).

[7]R. Freeman and G. Bjorklund, Phys. Rev. Lett. **40**, 118 (1978).

[8]S. M. Jaffe, R. Kachru, N. H. Tran, H. B. van Linden van den Heuvell, and T. F. Gallagher, Phys. Rev. A **30**, 1828 (1984).

[9]E. Salomon, J. Cooper, and D. Kelleher, Phys. Rev. Lett. **55**, 193 (1985).

[10]J. Neukammer, H. Rinneberg, G. Jonsson, W. E. Cooke, H. Hieronymus, A. Konig, K. Vietzke, and H. Spinger-Bolk, Phys. Rev. Lett. **55**, 1979 (1985).

[11]The three-day workshop at Gif-sur-Yvette in Orsay, France was organized by Mireille Aymar of Laboratoire Aime Cotton and Annick Giusti of Laboratoire Photophysique Moleculaire of Université Paris-Sud, Orsay.

[12]H. Friedrich and D. Wintgen, Phys. Rev. A **32**, 3231 (1985); J. Zaanen and G. A. Sawatzky, Phys. Rev. B **33**, 8074 (1986); S. Ravi and G. S. Agarwal, Phys. Rev. A **35**, 3291 (1987).

[13]P. McNicholl, J. Ivri and T. Bergeman (unpublished).

[14]M. Feldman, P. Lebow, F. Raab, and H. Metcalf, Appl. Opt. **17**, 774 (1978).

[15]M. G. Littman and H. J. Metcalf, Appl. Opt. **17**, 2224 (1978).

[16]P. McNicholl and H. J. Metcalf, Appl. Opt. **24**, 2757 (1985).

[17]It is curious to note that the decay of a spectral feature with a Fano line shape is also exponential.

[18]For the spectral features studied here, the decay rate is reduced by more than a factor of 500, and the region studied represents only the very narrow region near the minimum where it changes by less than a factor of 5 as shown in Fig. 6.

[19]D.-H. Yang (private communication). A paper in progress will discuss procedures for electric field mapping using stabilized states in the Stark effect.

[20]C. Kocher, Phys. Rev. A **6**, 35 (1972).

[21]W. Davis, H. Metcalf, and W. Phillips, Phys. Rev. A **19**, 700 (1979).

[22]J. Rubbmark, M. Kash, M. Littman, and D. Kleppner, Phys. Rev. A **23**, 3107 (1981).

[23]D. A. Harmin (private communication).

[24]D. A. Harmin, Phys. Rev. A **30**, 2413 (1984), Sec. V. See also K. Sakimoto, J. Phys. B **19**, 3011 (1986).

[25]P. Risberg, Ark. Fys. **10**, 583 (1956).

[26]P. Goy, C. Fabre, M. Gross, and S. Haroche, J. Phys. B **13**, L83 (1980); C. Fabre, S. Haroche, and P. Goy, Phys. Rev. A **22**, 778 (1980).

[27]T. F. Gallagher, R. M. Hill, and S. A. Edelstein, Phys. Rev. A **13**, 1448 (1976); **14**, 744 (1976).

[28]R. R. Freeman and D. Kleppner, Phys. Rev. A **14**, 1614 (1976).

[29]M. M. Salour, Opt. Commun. **18**, 377 (1976).

[30]W. E. Cooke and T. F. Gallagher, Phys. Rev. A **21**, 588 (1980); T. F. Gallagher, in *Rydberg States of Atoms and Molecules*, edited by R. F. Stebbings and F. B. Dunning (Cambridge University Press, Cambridge, England, 1982).

[31]J. W. Farley and W. H. Wing, Phys. Rev. A **23**, 2397 (1981).

[32]J. R. Hiskes, C. B. Tarter, and D. A. Moody, Phys. Rev. **133**, A424 (1964).

[33]C. Theodosiou, Phys. Rev. A **30**, 2881 (1984), and references cited therein.

[34]K. Omidvar, At. Data Nucl. Data Tables **28**, 1 (1982).